

# Physics Informed Neural Networks for Thermal Analysis of Laser Powder Bed Fusion Process

E. Hosseini<sup>a,\*</sup>, P. Gh Ghanbari<sup>a,b</sup>, O. Müller<sup>a,b</sup>, R. Molinaro<sup>c</sup>, S. Mishra<sup>d</sup>

<sup>a</sup>*Empa Swiss Federal Laboratories for Materials Science & Technology, Dübendorf, Switzerland*

<sup>b</sup>*Institute for Mechanical Systems, Department of Mechanical and Process Engineering, ETH Zürich, Switzerland*

<sup>c</sup>*Seminar for Applied Mathematics, Department of Mathematics, ETH Zürich, Switzerland*

<sup>d</sup>*Seminar for Applied Mathematics, Department of Mathematics and ETH AI Center, ETH Zürich, Switzerland*

---

## Abstract

The high computational cost of physics-based simulations is one of the main challenges in realising Digital Twins for complex systems such as metal additive manufacturing (MAM). Modelling the highly localised and rapid phenomena occurring during MAM processes such as laser powder bed fusion (LPBF) requires very fine time- and space-discretisations in classical simulation approaches such as the finite element method (FEM). Particularly, when the solution is required for a range of scenarios, e.g. in sensitivity or optimisation analyses, computation costs of such simulations is prohibitive. This study explores and adapts physics informed neural networks (PINNs) to the thermal analysis of the LPBF process, through which reliable and real-time outcomes can be achieved. An unsupervised learning strategy was employed to (parametrically) solve the heat transfer equation for the LPBF process. The trained network calculates the temperature profiles (and the melt-pool dimensions) evolving during the LPBF process for any given set of material's thermal properties and process conditions at practically zero computational cost. The reliability of PINNs was verified based on outcomes of several benchmark equivalent finite element simulations.

**Keywords:** Additive manufacturing, Thermal analysis, Physics informed neural networks, Parametric analysis

---

\*Corresponding author: E. Hosseini, ehsan.hosseini@empa.ch, Empa Swiss Federal Laboratories for Materials Science & Technology

## 1. Introduction

Marking its evolution as a central feature of the Fourth industrial revolution, additive manufacturing broadly refers to the layer-by-layer *printing* of spatially precise on-demand 3D objects with enhanced design freedom relative to conventional technologies. Effective contribution of metal additive manufacturing (MAM) to the vision of Industry 4.0 necessitates addressing its key challenges in the cost and reliability of the printed parts [1]. The cost barrier to extensive adoption of MAM technology inherently arises from both the high costs of the production process (e.g. due to slow manufacturing and expensive feed materials) and the high rate of manufacturing failures [2, 3]. The high production cost tends to move the application of the technology to specific cases where MAM can result in adequate value creation, i.e. fabrication of complex geometries, or where conventional manufacturing would be even more expensive, e.g. small batch production [4]. The most significant contributions to the cost of MAM originate from the difficulties in choosing the *right* printing process parameters where non-optimal conditions can result in inferior quality or total failure of the printing process [5]. This can be attributed to local overheating, excessive distortion, cracking, high porosity, undesired microstructure, or poor mechanical properties, to name a few [6, 7]. Currently, the state of the art strategy for optimizing the process parameters for a given printing machine, material or part involves a lot of trial and error, based on numerical experiments, leading to very high cost in terms of time as well as resources [3, 8, 9].

As a core component of Industry 4.0, Digital Twins provide a virtual duplicate of a system and can predict its state and outcome under various operating conditions based on a detailed understanding of its operating principles and accordingly provide guidance for maximising the system efficiency [10, 11, 12, 13]. Digital Twins in manufacturing systems integrate physics-based simulations and data-driven machine learning models with historical and real-time sensor information to actively learn and predict the state of the system and products [14]. When reliability and security are guaranteed, they can autonomously control and optimise the process and make ever-accurate real-time decisions [11, 12]. For MAM systems, Digital Twins are expected to enable a more systematic optimisation and control of the process conditions to achieve the goal of *first-time-right* high-quality production.

One of the main challenges in realising Digital Twins for complex processes such as MAM is the high computational cost of physics-based simulations, which impedes achieving reliable

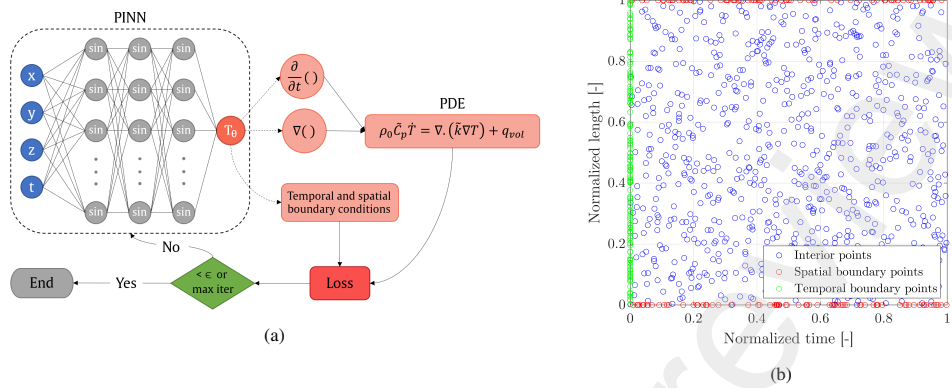


Figure 1: a) A schematic diagram of the physics informed neural network for solving the heat equations where the loss function contains a mismatch in the temporal and spacial boundary conditions and the residuals for the PDE on a set of collocation points in the time-space(-parameters) domain. b) low-discrepancy *Sobol* sampling for interior, spatial and temporal boundary collocation points.

real-time analyses [15]. MAM is a multi-physics field problem and requires different types of costly computer simulations, namely: thermal, mechanical, metallurgical, and fluid dynamics [16, 17, 18]. The underlying reason for the high computational cost of these simulations lies in the extremely rapid (in time) and small (in space) scales of the phenomena occurring during MAM processes [19]. As a result, classical numerical techniques such as the finite element method (FEM) require very fine discretisations (grids) to solve the governing partial differential equations (PDEs). To put this limitation into perspective, the temperature gradients and cooling rates in the vicinity of the process zone in the LPBF process can be in the orders of  $1 \times 10^6$  K/m and  $1 \times 10^6$  K/s [20, 21], which demands the adoption of micrometre-sized and microsecond-long space- and time-discretisation within the FEM framework, and therefore, does not allow for real-time analyses. Hence, it is imperative to develop alternative simulation strategies that will accelerate simulation time by orders of magnitude, while ensuring accuracy and robustness of the resulting simulation outputs.

To this end, this article explores and *adapts* recently proposed machine learning (AI) techniques, in the form of physics informed neural networks (PINNs), for developing reliable and rapid analysis strategies for LPBF, as an efficient alternative to the classical numerical methods. This study focuses on the thermal simulation of the process, as it is the most basic and fundamental analysis for LPBF whose outputs are necessary in other simulations such as (thermo)mechanical and metallurgical and ultimately in the development of Digital Twins.

Physics-informed neural networks (PINNs) are a class of deep neural networks that employ automatic differentiation to solve the governing PDEs of a system for a given set of temporal and spatial boundary conditions and represent its behaviour accordingly [22, 23] and references therein. The main advantage of PINNs over classical approaches such as FEM lies in their high computational efficiency and *their ability to serve as an ultrafast surrogate for solving parametric PDEs*. In contrast to common machine learning approaches that rely on a vast amount of data for training, PINNs can learn in an unsupervised fashion [24, 25, 23] and references therein.

The proposed PINNs in this study calculate the temperature profiles (and the melt-pool dimensions) during the LPBF process for any given set of the underlying material's thermal properties and process conditions at effectively zero computational cost. Two different PINNs for the thermal analysis of the LPBF process are presented. The first assumes a temperature-independent thermal behaviour for the material and solves the heat equation over a range of thermal conductivities, specific heat capacities and densities during LPBF with various values for the laser power and scanning speed. Moreover, to demonstrate the application of PINNs for temperature-dependent material properties, the second set of PINNs proposed here solve a (nonlinear) heat equation with consideration of the thermal response of Hastelloy X and represents the temperature profiles and the melt-pool dimensions during the LPBF process for any given combination of laser powers and scanning speeds. Both PINNs were verified based on outcomes of several equivalent finite element simulations in a benchmark study and were found extremely cheap computationally, while retaining accuracy.

## 2. Physics Informed Neural Networks (PINNs)

Partial differential equations (PDEs) describe the response of many natural and man-made phenomena in science and technology. As analytical solutions are only available for very special types and instances of PDEs, numerical simulation methods such as finite difference, finite element, and finite volume methods are generally employed for practical problems. Although successful in many cases, the computational cost of such numerical approaches for application to complex phenomena is prohibitively high, particularly for problems in which the solution to the PDEs is required for various scenarios [26, 27] and references therein, e.g. for sensitivity analysis, uncertainty quantification and optimisation problems in Digital Twins.

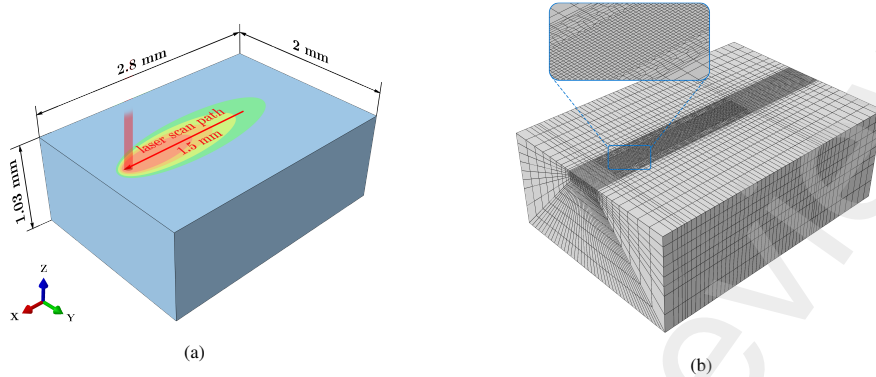


Figure 2: a) Details for the evaluated thermal problem, b) the designed mesh for the FE analysis using ABAQUS [5].

In the past few years, machine learning has emerged as a central tool in scientific computing, and deep learning is considered an effective method for the numerical approximation of PDEs [23] and references therein. In this context, deep neural networks (DNNs) possess the so-called universal approximation property or the ability to approximate any continuous function and, therefore, can be the ansatz space for the solutions of PDEs [28]. This was the underlying idea of PINNs, first proposed by Lagaris et al. [29, 30], see also [31], and revived and further developed recently by Karniadakis and collaborators [32, 33], to cite just a few, and we refer the readers to [23] for a review. In contrast to the conventional machine learning tools in data science, which require large amounts of labelled data-sets, training of PINNs does not necessarily need any labelled data-sets, and PINNs can be purely thought of as unsupervised learners [34] for solving PDEs. Nevertheless, the flexibility of PINNs does incorporate labelled data when available (for more information regarding semi-supervised PINNs refer to Raissi et al. [22]).

Assuming the example of thermal simulation of LPBF process, it is desired to solve the governing PDE, written in abstract notation as  $D(T) = f$  (heat equation), and determine  $T$  (temperature field) as a function of  $y$  (space, time, and material/process parameters) such it satisfies the given temporal and spatial boundary conditions, written as  $B(T) = g$ . We describe how PINNs can be used to approximate this PDE below.

A feed-forward DNN might be considered to transform input  $y$  to output  $T$  through layers of neurons, which are composed of affine-linear maps between neurons in successive layers and a scalar nonlinear activation function [35]. Mathematically and for the shown  $K$ -layer DNN in

Fig. 1a [25]:

$$T_\theta(\mathbf{y}) = C_K \circ \sigma \circ C_{K-1} \circ \dots \circ \sigma \circ C_2 \circ \sigma \circ C_1(\mathbf{y}) \quad (1)$$

where  $\circ$  refers to the composition of functions. The network has  $K - 1$  hidden layers where  $k^{th}$  hidden layer transforms an input vector  $z_k$  by an affine linear function  $C_k$ , i.e.  $C_k(z_k) = W_k z_k + b_k$ , and then by a scalar (nonlinear) activation function  $\sigma$  (*logistic*, *sin*, *tanh*, etc. [35]). Training of DNNs is searching for the best concatenated set of tuning parameters  $\theta = \{W_k, b_k\}$  using gradient descent methods such that the mismatch between the neural network and the underlying target is minimised [25].

Within the PINNs framework,  $T_\theta$  is the approximate solution of the PDE  $D(T) = f$  and therefore, the tuning parameters should be found to minimise the following residual [29, 25].

$$R_{PDE,\theta} = D(T_\theta) - f \quad (2)$$

Additionally, the solution should satisfy the initial and boundary conditions of the problem, requiring us to minimize the following *boundary* residual,

$$R_{BC,\theta} = B(T_\theta) - g. \quad (3)$$

PINN is a grid-free approach. Hence, we need to evaluate and minimise, on average, the residuals for a chosen set of *collocation* points  $\{\mathbf{y}_n\}$ , see Fig. 1b. Commonly, the low-discrepancy *Sobol* sampling strategy is adapted for creating the collocation point set [36, 37], while it was found in this study that a more clever sampling strategy, inspired by the physics of the problem, can significantly improve the learning efficiency.

Eventually, training a PINN involves finding the set of optimal parameters  $\theta^*$  such that [25]:

$$\theta^* = \operatorname{argmin}_\theta (\|R_{PDE,\theta}\| + \lambda \|R_{BC,\theta}\|) \quad (4)$$

The solution of the above minimisation problem does not necessitate access to *labelled training data* and can be seen as an *unsupervised* learning algorithm.

Coding and implementation of PINNs, e.g. within the *PyTorch* framework, is extremely simple and only needs a few lines of Python code. In contrast to the classical simulation approaches based on numerical schemes for differentiation, PINNs employ differential operators on graphs and uses GPU-accelerated automatic differentiation to elegantly and efficiently calculate the differential operators of the governing equations and those required in the gradient descent method

for the training of the neural networks [38, 39]. Importantly, PINNs are very well suited for solving parametric PDEs [40], i.e. when the solution to the governing PDE is required for different scenarios (e.g. different material parameters and process conditions for thermal analysis of the LPBF process). A solution to such a problem through classical numerical solvers needs individual simulations for each scenario and is prohibitively costly. Finally, PINNs have the added advantage of being equipped with rigorous convergence and error control guarantees for a large spectrum of PDEs, see [25, 24, 41, 42] and references therein. These rigorous bounds provide further rationale for the deployment in PINNs in a variety of contexts in scientific computing.

### 3. PINNs for Thermal Analysis of LPBF Process

In this study, the main objective is calculating the transient and steady-state temperature profiles (and melt pool dimensions) during the LPBF process for any given process parameters and the underlying material's thermal properties. It is well known that the induced temperature profiles by the laser stabilise after <1.5 mm from the start of a track in the LPBF process [43]. Therefore, to include both transient and steady thermal states, analyses were conducted for a 1.5 mm long laser track within a large enough domain with the dimensions of 2.8 mm × 2.0 mm × 1.0 mm (L×W×H), Fig. 2a.

Following [44, 45, 46], this study employed the continuum thermal modelling strategy for the analysis of the LPBF process. This method makes simplifications such as ignoring phenomena related to explicit modelling of individual powder particles or molten metal motion in the analysis to moderate its computational cost. The primary heat transfer mechanism is assumed to be conduction, and heat loss due to convection and radiation is neglected, similar to [47]. Accordingly, a time-dependent temperature field  $T(x, y, z, t, \dots)$  is sought to satisfy the thermal energy conservation equation (and the given temporal and spatial boundary conditions):

$$\rho_0 \tilde{C}_p \dot{T} = \nabla \cdot (\tilde{k} \nabla T) + q_{vol} \quad (5)$$

Here  $\rho_0$ ,  $\tilde{C}_p$  and  $\tilde{k}$  are the reference density, apparent specific heat capacity, and effective thermal conductivity, respectively, and  $q_{vol}$  is the volumetric heat generation term representing the contribution of laser energy source. The apparent specific heat capacity is a temperature-dependent quantity that deviates from the material's specific heat capacity  $C_p$  in the temperature ranges relevant to a phase transformation to account for the associated enthalpy changes [48]. The effective

thermal conductivity is also a temperature-dependent quantity that deviates from the material's thermal conductivity  $k$  at temperatures higher than the melting point to account for the heat distribution induced by convection of molten metal due to Marangoni and buoyancy mechanisms [49, 46].

The volumetric heat generation term  $q_{vol}$  in Eq. 5 can be considered as a semi-spherical shape heat source centred at the location of the laser [49, 50]:

$$q_{vol} = \alpha \frac{6\sqrt{3}P}{\pi \sqrt{\pi}r^3} \exp\left(-3\frac{(x+vt)^2 + y^2}{r^2}\right) \exp\left(-3\frac{z^2}{c^2}\right) \quad (6)$$

where  $P$  is the laser power,  $\alpha$  is the laser absorption coefficient,  $r$  is the laser radius,  $c$  is the laser penetration depth, and  $v$  is the laser scan speed (discussions on more advanced formulations for considering the laser heat source can be found in [51]).

Solving the above problem for a given set of process and material parameters through FEM is straightforward and was used in this study to establish the *ground truth* results for evaluating the PINNs solutions. As shown in Fig. 2b, an optimised mesh was generated which employs small elements only in the vicinity of the laser path to increase the efficiency of the computations [5]. The model has 110k nodes and 102k elements with the characteristic grid size of 10  $\mu\text{m}$  close to the laser path and up to 150  $\mu\text{m}$  elements on the outer boundaries of the domain. The FE solution of the above problem using 12 threads of an Intel Xeon Gold 6150 CPU took  $\sim 0.2$  h and  $\sim 2.5$  h without and with consideration of temperature dependence of the material's thermal properties, respectively. The consideration of temperature-dependent thermal properties introduces nonlinearities that necessitate the adoption of smaller time increments and more iterations for the solver to converge, which leads to higher computational costs. It is evident that FEM can be used neither for generating real-time simulation data for a Digital Twin nor in sensitivity analyses where the solution for a large span of process and material parameters is required.

In this study, we aim to use PINNs as an alternative strategy for thermal analysis of LBPF and obtain a generalised (parametric) solution for Eq. 5 which provides the temperatures not only as a function of time and space but also as a function of process and material parameters, namely laser power, absorption coefficient, laser scan speed, density, conductivity, and heat capacity. It can be deduced from Eqs. 5 & 6 that the effect of laser power and absorption coefficient, as well as that for heat capacity and density, are coupled and therefore can be combined into single parameters for the generalised solution of Eq. 5.

Fig. 3 illustrates a schematic of the proposed PINNs for the thermal analysis of the LPBF

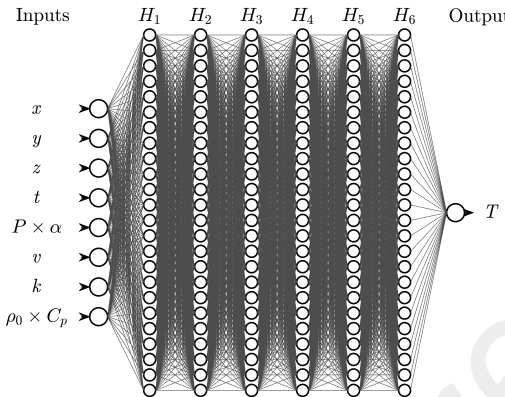


Figure 3: Schematics of the developed PINNs for the thermal analysis of the LPBF process [54].

process. A fully connected feed-forward neural network with six hidden layers of 24 neurons each with  $\sin$  activation functions was constructed. The network takes eight inputs being: three space coordinates, time, laser power  $\times$  absorption coefficient, laser scanning speed, effective thermal conductivity, and apparent specific heat capacity  $\times$  reference density, and provides the temperature as the output. Training the network involved optimising the weights and biases (ca. 3K unknown values) based on the LBFGS algorithm [52] in order to minimize the residuals associated with the PDE as well as temporal and spatial boundary conditions, collocated on  $2^{19}$  collocation points. The choice of collocation points is vital to the efficiency and accuracy of PINNs in this context and *constitutes a key innovation in this paper, when compared to plain vanilla PINNs*. In particular, we propose a nonhomogeneous distribution of the interior collocation points such that a higher point population exists in the vicinity of the laser heat source, where higher temperature gradients are expected. For such a purpose, a random Spherical collocation point distribution [53], centred at the location of the moving heat source and with a radius of 300  $\mu\text{m}$ , was adopted for 10% of the interior collocation points (Fig. 4b). This distribution was superimposed on a Cartesian *Sobol* collocation point distribution (Fig. 4a) to construct the interior collocation point set used for calculation of  $R_{PDE}$ , as presented in Fig. 4c.

The network was trained for two scenarios. PINNs-I were trained without consideration of the temperature dependence of the material's thermal properties to estimate temperature as  $T = T(x, y, z, t, P \times \alpha, v, k, \rho_0 \times C_p)$ . To demonstrate the capability of PINNs for thermal analysis of LPBF process with consideration of temperature-dependent material properties and taking

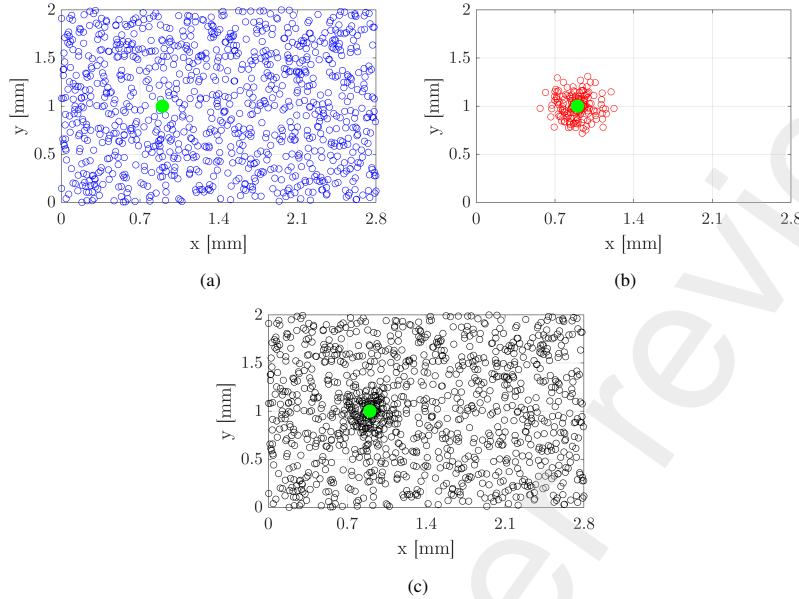


Figure 4: a ) Low-discrepancy Cartesian *Sobol* sampling, b) random Spherical collocation point sampling, centred at the location of the moving heat source, c) superposition of samplings shown in (a) and (b) to form the adopted interior collocation points for PINNs. Note that the green circle presents the temporal location of the laser heat source.

into account the strong nonlinearities of the apparent specific heat capacity and effective thermal conductivity, the shown thermal properties of LPBF Hastelloy X in Fig. 5 were employed to train PINNs-II and calculate the temperature profile as  $T = T(x, y, z, t, P \times \alpha, v)$ . The outcomes of PINNs-II were also assessed to calculate the dimensions of meltpool i.e.  $D_{meltpool} = D_{meltpool}(P \times \alpha, v)$ .

The models and scripts used in this study are available on [Github](#). Training of PINNs was performed on a single Nvidia Titan RTX GPU and took  $\sim 1.8$  h and  $\sim 4$  h for PINNs-I and PINNs-

Table 1: Training and benchmark evaluation conditions for PINNs-I.

Parameter Unit	$K$ [ $\text{WK}^{-1}$ ]	$\rho_0 \times C_p$ [ $\text{mJm}^{-3}\text{K}^{-1}$ ]	$P \times \alpha$ [W]	$v$ [ $\text{ms}^{-1}$ ]
Training range	5 - 20	2-5	10-20	0.5-1.5
Benchmark # 1	13.30	2.65	18.84	0.87
Benchmark # 2	8.14	3.86	15.08	0.80
Benchmark # 3	10.86	2.45	12.60	1.09
Benchmark # 4	7.07	4.59	17.70	1.23
Benchmark # 5	19.02	4.48	11.61	0.59
Benchmark # 6	15.61	3.48	14.47	1.37

II, respectively. After the training, i.e., at the time of *inference*, the evaluation of networks for calculating temperature profiles for any combination of process and material parameters is at practically zero computational cost which makes them ideal for real-time simulations and ultimately control and optimisation of the LPBF process within a Digital Twin framework. The computational cost of a single PINNs evaluation was  $\sim 120\text{ }\mu\text{s}$ . For each of the presented benchmark cases, it took 20 ms to evaluate PINNs 1.75 million times (in parallel) and create similar data sets to those from FE analysis which indicated that PINNs were 5-6 orders of magnitudes faster than the FE method. Another major advantage of PINNs over FEM is the very small disk-size (storage) of the final solution, which is a couple of megabytes for the whole range of process-material parameters for the former, but can be upwards of a gigabyte for every single scenario for FEM simulations.

The verification of the PINNs solution in this study was based on comparing the outcome with those from several benchmark equivalent FEM simulations. A *hypercube* sampling strategy [55] was used to design six benchmarking cases. Tables 1 and 2 describe the training ranges of the two PINNs as well as the conditions for their benchmark evaluation.

#### 4. Benchmark Evaluation

This section provides the results of the benchmark evaluation of the two established PINNs solutions for thermal analysis of the LPBF process. The relative Mean Absolute Error (MAE) was employed as an index in the assessment of the accuracy of PINNs solutions, i.e.:

$$\bar{\delta} = \left( \frac{|T_{PINNs} - T_{FEM}|}{|T_{FEM}|} \right) \times 100 \quad (7)$$

Table 2: Training and benchmark evaluation conditions for PINNs-II.

Parameter Unit	$P \times \alpha$ [W]	$v$ [ms $^{-1}$ ]
Training range	50-100	0.5-1.5
Benchmark # 1	94.45	1.00
Benchmark # 2	71.52	0.55
Benchmark # 3	60.83	0.98
Benchmark # 4	87.18	1.47
Benchmark # 5	80.82	0.80
Benchmark # 6	50.14	1.22

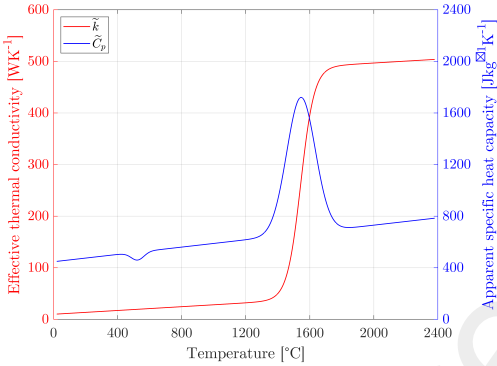


Figure 5: Thermal properties of LPBF Hastelloy X [56].

where the overline bar refers to the average of the underlying quantity computed over the set of FEM physical coordinates and operational conditions. Fig. 6 compares the PINNs-I and FE calculated transient and steady-state temperature data for the conducted benchmark evaluations. As can be seen, PINNs could provide a close approximation of the FEM results, where the MAE always remains below 4.5%.

Fig. 7 illustrates the PINNs-II calculated transient and steady-state temperature data and melt pool dimensions versus those derived from the equivalent FEM simulations. It can be observed from Figs. 6c & 6d and Figs. 7c & 7c that consideration of the temperature-dependent material properties significantly influenced the shape of the temperature profiles. Similar to that for PINNs-I, the observations from Fig. 7 indicate that PINNs-II could acceptably represent the outcomes of FEM simulations for the conducted benchmark evaluations. Even with the additional physics in the form of temperature dependent material properties leading to nonlinear feedback, the errors with PINNs was still below 4.5% and comparable to the first case.

## 5. Concluding Remarks

Reliable real-time simulation tools are required for realising Digital Twins for metal additive manufacturing (MAM) systems to better control and optimise the process conditions and improve the process efficiency and quality of the builds. However, the high computational cost of classical simulation approaches such as the finite element method for analysing the MAM process prohibits their exploitation to this end. This study developed a reliable and rapid alternative for thermal analysis of the laser powder bed fusion (LPBF) process based on physics

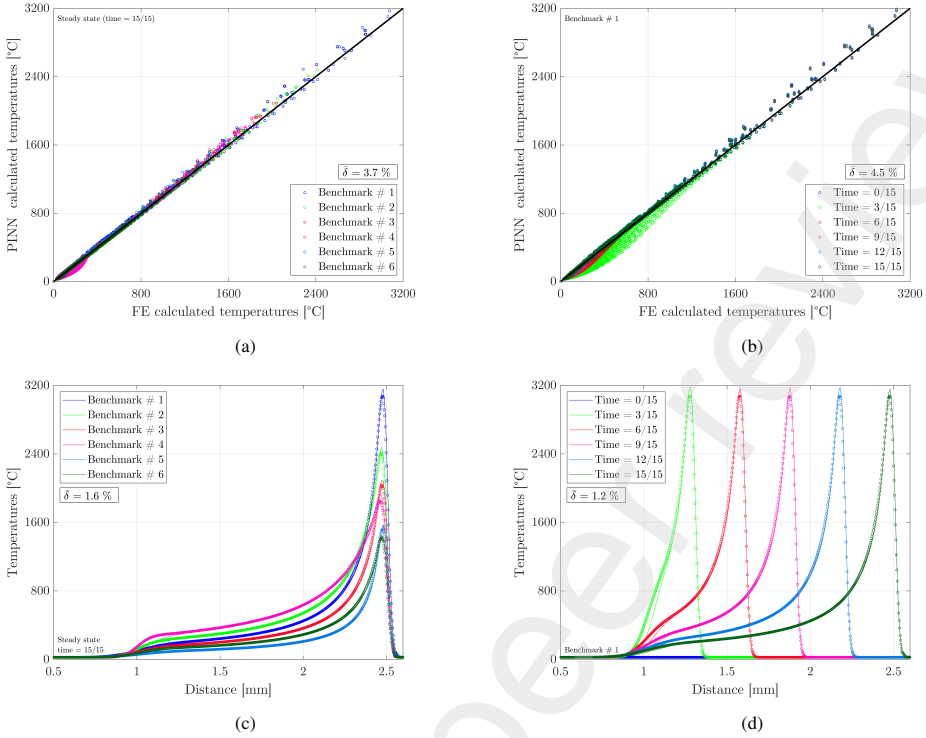


Figure 6: Comparison of calculated temperatures from PINNs-I and corresponding FEM simulations in benchmark cases. a) steady-state temperature distributions in six cases, b) transient and steady-state temperatures for the first benchmark, c) temperature profiles along the laser path for the last frame of analysis for the six cases, d) evolution of temperature profile along the laser path in the first case.

informed neural networks (PINNs). The outstanding advantage of the developed PINNs solutions is that, after unsupervised training, they calculate the transient and steady temperature profiles (and consequently the melt-pool dimensions) during the LPBF process for any combination of the material's thermal properties and process conditions at practically zero computational cost. A benchmark study ultimately compared the outcomes of the developed PINNs with those from a series of equivalent FEM simulations and indicated Mean Absolute Error of below 4.5% for PINNs approximations.

### Acknowledgments

Financial support by the Swiss National Science Foundation (SNSF; grant number 200551) is gratefully acknowledged. The research of RM and SM was partly performed under a project that has received funding from the European Research Council (ERC) under the European Union's

Horizon 2020 research and innovation programme (grant agreement No. 770880).

## Supplementary Materials

The models and scripts used in this study can be downloaded from on [Github](#).

## References

- [1] Mahesh Mani, Shaw Feng, Brandon Lane, Alkan Donmez, Shawn Moylan, and Ronnie Fesperman. Measurement science needs for real-time control of additive manufacturing powder bed fusion processes. 2015.
- [2] Jonas Barsing. A cost breakdown and production uncertainty analysis of additive manufacturing: A study of low-volume components produced with selective laser melting, 2018.
- [3] T DebRoy, T Mukherjee, JO Milewski, JW Elmer, B Ribic, JJ Blecher, and W Zhang. Scientific, technological and economic issues in metal printing and their solutions. *Nature materials*, 18(10):1026–1032, 2019.
- [4] Simon Ford and Mélanie Despesesse. Additive manufacturing and sustainability: an exploratory study of the advantages and challenges. *Journal of cleaner Production*, 137:1573–1587, 2016.
- [5] William J Sames, FA List, Sreekanth Pannala, Ryan R Dehoff, and Sudarsanam Suresh Babu. The metallurgy and processing science of metal additive manufacturing. *International materials reviews*, 61(5):315–360, 2016.
- [6] Dong Dong Gu, Wilhelm Meiners, Konrad Wissenbach, and Reinhart Poprawe. Laser additive manufacturing of metallic components: materials, processes and mechanisms. *International materials reviews*, 57(3):133–164, 2012.
- [7] E Hosseini and VA Popovich. A review of mechanical properties of additively manufactured inconel 718. *Additive Manufacturing*, 30:100877, 2019.
- [8] Tridibesh Mukherjee and Tarasankar DebRoy. A digital twin for rapid qualification of 3d printed metallic components. *Applied Materials Today*, 14:59–65, 2019.
- [9] Ian Gibson, David W Rosen, Brent Stucker, Mahyar Khorasani, David Rosen, Brent Stucker, and Mahyar Khorasani. *Additive manufacturing technologies*, volume 17. Springer, 2021.
- [10] Edward Glaessgen and David Stargel. The digital twin paradigm for future nasa and us air force vehicles. In *53rd AIAA/ASME/ASCE/AHS/ASC structures, structural dynamics and materials conference 20th AIAA/ASME/AHS adaptive structures conference 14th AIAA*, page 1818, 2012.
- [11] Diego M Botín-Sanabria, Adriana-Simona Mihaita, Rodrigo E Peimbert-García, Mauricio A Ramírez-Moreno, Ricardo A Ramírez-Mendoza, and Jorge de J Lozoya-Santos. Digital twin technology challenges and applications: A comprehensive review. *Remote Sensing*, 14(6):1335, 2022.
- [12] Maulshree Singh, Evert Fuenmayor, Eoin P Hinchy, Yuansong Qiao, Niall Murray, and Declan Devine. Digital twin: Origin to future. *Applied System Innovation*, 4(2):36, 2021.
- [13] Roberto Molinaro, Joel-Steven Singh, Sotiris Catsoulis, Chidambaram Narayanan, and Djamel Lakehal. Embedding data analytics and cfd into the digital twin concept. *Computers&Fluids*, 214:104759, 2021.
- [14] Florian Jaensch, Akos Csiszar, Christian Scheifele, and Alexander Verl. Digital twins of manufacturing systems as a base for machine learning. In *2018 25th International Conference on Mechatronics and Machine Vision in Practice (M2VIP)*, pages 1–6. IEEE, 2018.
- [15] Lihang Yang and Tuğrul Öznel. Physics-based simulation models for digital twin development in laser powder bed fusion. *International Journal of Mechatronics and Manufacturing Systems*, 14(2):143–163, 2021.
- [16] HL Wei, T Mukherjee, W Zhang, JS Zuback, GL Knapp, A De, and T DebRoy. Mechanistic models for additive manufacturing of metallic components. *Progress in Materials Science*, 116:100703, 2021.
- [17] Wentao Yan, Stephen Lin, Orion L Kafka, Yanping Lian, Cheng Yu, Zeliang Liu, Jinhui Yan, Sarah Wolff, Hao Wu, Ebot Ndip-Agbor, et al. Data-driven multi-scale multi-physics models to derive process–structure–property relationships for additive manufacturing. *Computational Mechanics*, 61(5):521–541, 2018.
- [18] Rishi Ganeriwala and Tarek I Zohdi. Multiphysics modeling and simulation of selective laser sintering manufacturing processes. *Procedia Cirp*, 14:299–304, 2014.
- [19] P Gh Ghanbari, Edoardo Mazza, and Ehsan Hosseini. Adaptive local-global multiscale approach for thermal simulation of the selective laser melting process. *Additive Manufacturing*, 36:101518, 2020.
- [20] HK Rafi, NV Karthik, Haijun Gong, Thomas L Starr, and Brent E Stucker. Microstructures and mechanical properties of ti6al4v parts fabricated by selective laser melting and electron beam melting. *Journal of materials engineering and performance*, 22(12):3872–3883, 2013.
- [21] Neil J Harrison, Iain Todd, and Kamran Mumtaz. Reduction of micro-cracking in nickel superalloys processed by selective laser melting: A fundamental alloy design approach. *Acta Materialia*, 94:59–68, 2015.

- [22] Maziar Raissi, Paris Perdikaris, and George E Karniadakis. Physics-informed neural networks: A deep learning framework for solving forward and inverse problems involving nonlinear partial differential equations. *Journal of Computational physics*, 378:686–707, 2019.
- [23] Salvatore Cuomo, Vincenzo Schiano Di Cola, Fabio Giampaolo, Gianluigi Rozza, Maizar Raissi, and Francesco Piccialli. Scientific machine learning through physics-informed neural networks: Where we are and what's next. *arXiv preprint arXiv:2201.05624*, 2022.
- [24] Siddhartha Mishra and Roberto Molinaro. Estimates on the generalization error of physics-informed neural networks for approximating a class of inverse problems for pdes. *IMA Journal of Numerical Analysis*, 42(2):981–1022, 2022.
- [25] Siddhartha Mishra and Roberto Molinaro. Estimates on the generalization error of physics-informed neural networks for approximating pdes. *IMA Journal of Numerical Analysis*, 2022.
- [26] Kjetil O Lye, Siddhartha Mishra, and Deep Ray. Deep learning observables in computational fluid dynamics. *Journal of Computational Physics*, page 109339, 2020.
- [27] Kjetil O Lye, Siddhartha Mishra, Deep Ray, and Praveen Chandrashekhar. Iterative surrogate model optimization (ISMO): An active learning algorithm for PDE constrained optimization with deep neural networks. *Computer Methods in Applied Mechanics and Engineering*, 374:113575, 2021.
- [28] Kurt Hornik, Maxwell Stinchcombe, and Halbert White. Multilayer feedforward networks are universal approximators. *Neural networks*, 2(5):359–366, 1989.
- [29] Isaac E Lagaris, Aristidis Likas, and Dimitrios I Fotiadis. Artificial neural networks for solving ordinary and partial differential equations. *IEEE transactions on neural networks*, 9(5):987–1000, 1998.
- [30] Isaac E Lagaris, Aristidis C Likas, and Dimitris G Papageorgiou. Neural-network methods for boundary value problems with irregular boundaries. *IEEE Transactions on Neural Networks*, 11(5):1041–1049, 2000.
- [31] MWMG Dissanayake and N Phan-Thien. Neural-network-based approximations for solving partial differential equations. *Communications in Numerical Methods in Engineering*, 1994.
- [32] Maziar Raissi and George Em Karniadakis. Hidden physics models: Machine learning of nonlinear partial differential equations. *Journal of Computational Physics*, 357:125–141, 2018.
- [33] Zhiping Mao, Ameya D Jagtap, and George Em Karniadakis. Physics-informed neural networks for high-speed flows. *Computer Methods in Applied Mechanics and Engineering*, 360:112789, 2020.
- [34] Mehryar Mohri, Afshin Rostamizadeh, and Ameet Talwalkar. *Foundations of machine learning*. MIT press, 2018.
- [35] Ian Goodfellow, Yoshua Bengio, and Aaron Courville. *Deep learning*. MIT press, 2016.
- [36] Russel E Caflisch. Monte carlo and quasi-monte carlo methods. *Acta numerica*, 7:1–49, 1998.
- [37] Siddhartha Mishra and T Konstantin Rusch. Enhancing accuracy of deep learning algorithms by training with low-discrepancy sequences. *SIAM Journal on Numerical Analysis*, 59(3):1811–1834, 2021.
- [38] Atilim Gunes Baydin, Barak A Pearlmutter, Alexey Andreyevich Radul, and Jeffrey Mark Siskind. Automatic differentiation in machine learning: a survey. *Journal of Machine Learning Research*, 18:1–43, 2018.
- [39] Stefano Markidis. The old and the new: Can physics-informed deep-learning replace traditional linear solvers? *Frontiers in big Data*, page 92, 2021.
- [40] Andrés Beltrán-Pulido, Ilias Bilionis, and Dionysios Aliprantis. Physics-informed neural networks for solving parametric magnetostatic problems. *IEEE Transactions on Energy Conversion*, 2022.
- [41] Tim De Ryck and Siddhartha Mishra. Error analysis for physics informed neural networks (PINNs) approximating Kolmogorov PDEs. *arXiv preprint arXiv:2106.14473*, 2021.
- [42] Tim De Ryck, Ameya D Jagtap, and Siddhartha Mishra. Error estimates for physics informed neural networks approximating the Navier-Stokes equations. *arXiv preprint arXiv:2203.09346*, 2022.
- [43] Subin Shrestha and Kevin Chou. A study of transient and steady-state regions from single-track deposition in laser powder bed fusion. *Journal of Manufacturing Processes*, 61:226–235, 2021.
- [44] Erik R Denlinger, Vijay Jagdale, GV Srinivasan, Tahany El-Wardany, and Pan Michaleris. Thermal modeling of inconel 718 processed with powder bed fusion and experimental validation using in situ measurements. *Additive Manufacturing*, 11:7–15, 2016.
- [45] Daniel Moser, Michael Cullinan, and Jayathi Murthy. Multi-scale computational modeling of residual stress in selective laser melting with uncertainty quantification. *Additive Manufacturing*, 29:100770, 2019.
- [46] Zhibo Luo and Yaoyao Zhao. Efficient thermal finite element modeling of selective laser melting of inconel 718. *Computational Mechanics*, 65(3):763–787, 2020.
- [47] Andrew J Pinkerton and Lin Li. Modelling the geometry of a moving laser melt pool and deposition track via energy and mass balances. *Journal of Physics D: Applied Physics*, 37(14):1885, 2004.
- [48] Ning An, Guangyu Yang, Kun Yang, Jian Wang, Meie Li, and Jinxiong Zhou. Implementation of abaqus user subroutines and plugin for thermal analysis of powder-bed electron-beam-melting additive manufacturing process. *Materials Today Communications*, 27:102307, 2021.
- [49] John Goldak, Aditya Chakravarti, and Malcolm Bibby. A new finite element model for welding heat sources. *Metallurgical transactions B*, 15(2):299–305, 1984.

- [50] John Goldak, M Bibby, J Moore, R House, and B Patel. Computer modeling of heat flow in welds. *Metallurgical transactions B*, 17(3):587–600, 1986.
- [51] Zhidong Zhang, Yuze Huang, Adhitian Rani Kasinathan, Shahriar Imani Shahabad, Usman Ali, Yahya Mahmood-khani, and Ehsan Toyserkani. 3-dimensional heat transfer modeling for laser powder-bed fusion additive manufacturing with volumetric heat sources based on varied thermal conductivity and absorptivity. *Optics & Laser Technology*, 109:297–312, 2019.
- [52] Dong C Liu and Jorge Nocedal. On the limited memory bfgs method for large scale optimization. *Mathematical programming*, 45(1):503–528, 1989.
- [53] Jan Morez, Jan Sijbers, Floris Vanhevel, and Ben Jeurissen. Constrained spherical deconvolution of nonspherically sampled diffusion mri data. *Human Brain Mapping*, 42(2):521–538, 2021.
- [54] Fabricio Castro. Artificial neural network architecture generator. *MATLAB Central File Exchange*, 2022.
- [55] Michael D McKay, Richard J Beckman, and William J Conover. A comparison of three methods for selecting values of input variables in the analysis of output from a computer code. *Technometrics*, 42(1):55–61, 2000.
- [56] Pooriya Gh Ghanbari, Rafal Wrobel, Bastian Rheingans, Thomas Mayer, Leinenbach Christian, Edoardo Mazza, and Ehsan Hosseini. Towards reliable and efficient 3d finite element thermal analysis of laser powder-bed fusion. *under review*, 2022.

## Highlights

- PINNs can be employed as robust and reliable approximators for (parametric) PDEs and as an alternative to methods such as FEM.
- PINNs were trained (without using any labelled data) for thermal analysis of the LPBF process for different material's thermal properties and process conditions.
- A novel *non-homogeneous* collocation point selection strategy was proposed to increase the efficiency and accuracy of PINNs.
- The reliability of the PINNs outcomes was verified based on the outcomes of several benchmark equivalent finite element simulations.
- The possibility of real-time thermal analysis through PINNS is essential for the control and optimisation of the LPBF process within the Digital Twins framework.

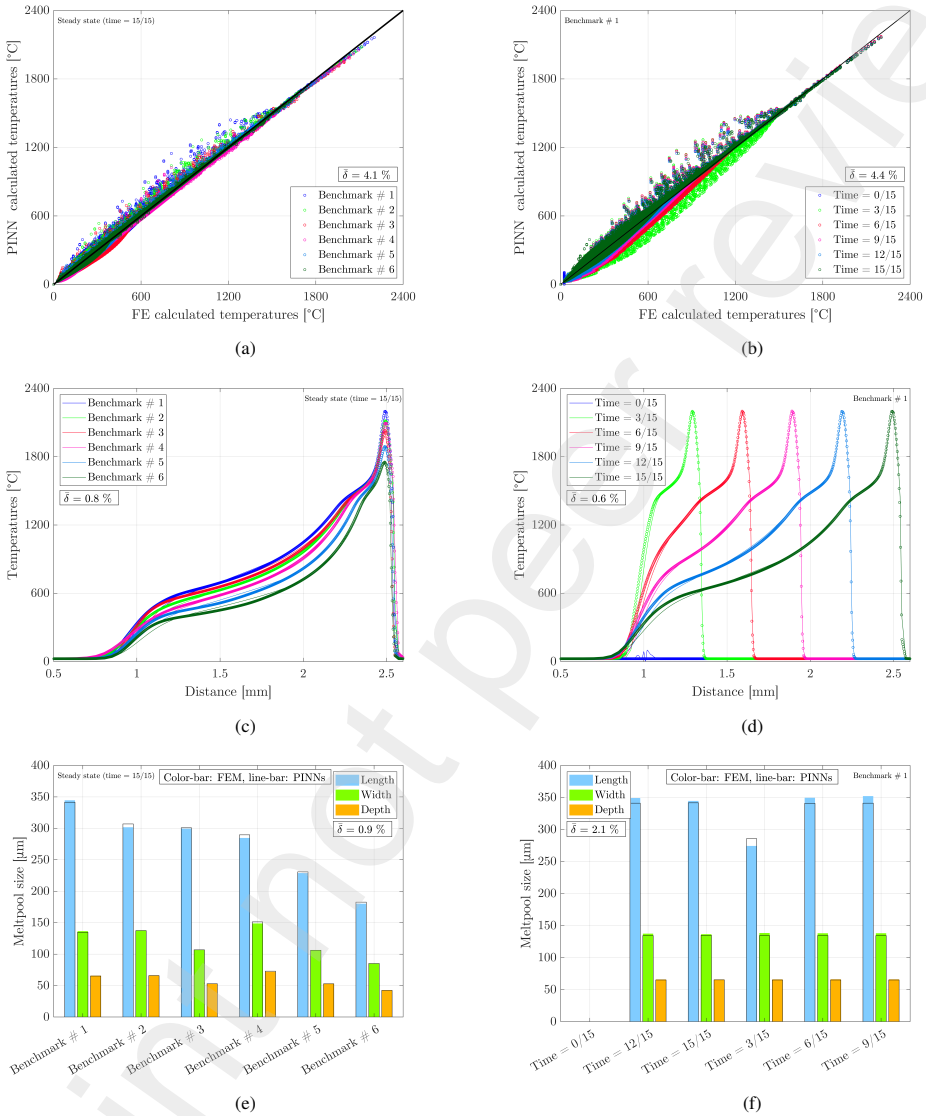


Figure 7: Comparison of calculated temperatures and melt pool dimensions from PINNs-II and corresponding FEM simulations in benchmark cases. a) steady state temperature distributions in six cases, b) transient and steady-state temperatures for the first benchmark, c) temperature profiles along the laser path for the last frame of analysis for the six cases, d) evolution of temperature profile along the laser path in the first case, e) steady-state melt pool dimensions for the six cases, f) evolution of melt pool size in the first benchmark case.